We are IntechOpen,
the world's leading publisher of
Open Access books
Built by scientists, for scientists

6,900
Open access books available

185,000
International authors and editors

200M
Downloads

154
Countries delivered to

Our authors are among the

TOP 1%
most cited scientists

12.2%
Contributors from top 500 universities

BOOK CITATION INDEX
CLARIVATE ANALYTICS
INDEXED

WEB OF SCIENCE™

Selection of our books indexed in the Book Citation Index
in Web of Science™ Core Collection (BKCI)

Interested in publishing with us?
Contact book.department@intechopen.com

A Finite Element Method Model for Large Strains Analysis of Timber

Vincenzo De Luca

Abstract

In this report a Finite Element Method (FEM) model, within the continuum mechanics of solids, for mechanical long term response of timber structures is presented. The proposed model can analyze three-dimensional solids, within the theory for non-linear material orthotropic elastic-viscous-plastic. It can account ductile behaviour in compression and brittle behaviour in tension, under the kinematics hypothesis of large displacements and large strains. The work has been carried out with a general purpose FEM software code in which a specific stress-strain law for wood, by a proper subroutine, has been built in. The constitutive equations have been formulated by a multi-surface yield approach of viscoplasticity, each yield surface acts separately each other. This approach is specifically almost necessary for some problems, such as glued composite parts or steel bolt connections. Specialized solution algorithms, which adopt time-stepping and automating relaxation techniques, have been used to handle the behaviour of the loading path response for elastic-viscous-plastic or elastic-brittle behaviours. The model has been applied to examples to test the effectiveness of the suggested approach. The results obtained have shown the potentiality of the proposed model to effectively simulate the overall mechanical behaviour of timber.

Keywords: finite element method, timber model, elasto-visco-plastic model, multi-surface yield visco-plasticity

1. Introduction

Wood is one of the ancient materials employed in construction. It is commonly used as parts in buildings, such as bridges, roofs, sports halls, and floors. Today timber, especially in the glue-laminated technology, is frequently used in new constructions. Wood, as a material in the

construction industry, has encountered a returned interest, mainly for its renewable nature, environmental compatibility and for its low energetic cost of production in comparison with concrete and steel.

Timber is advantageous, compared to other common construction materials, in wide spanning structures for its high ratio between load-carrying capacity and self-weight, along the longitudinal direction of grain. Timber structures have a good performance under dynamic loads for their elevated damping capacity. Although timber exhibits a consistent strength in the longitudinal direction for bending elements, in contrast it demonstrates a low value of tensile strength along the radial and tangential directions. This feature is unfavourable for connections, subjected to stress concentrations of tension, which can lead to crack development. However, timber is subjected to natural decay and its mechanical properties are sensitive to temperature and moisture.

An adequate mechanical description of timber material is an important task in scientific research on structural analysis of timber building. Also, an accurate stress analysis is particularly necessary for a composite system such as reinforced timber or pre-stressed timber, for the coupling and interaction of adhesive, lamination and reinforcements [1], and also for components used in connection joint [2].

In the scientific literature, many studies on modelling mechanics of wood can be retrieved [3]. However, continuum mechanics is the most common approach, being the basis of the finite element method (FEM) implementation. Within the theory of continuum mechanics, wood is assumed as an ideal homogeneous continuum [3], avoiding its complex nature. Wood is generally schematized as orthotropic elastic with three orthogonal material directions, corresponding to its longitudinal, radial and tangential growth fibre directions [3, 4]. However, experimental evidence [5] demonstrated that the extension of the Hooke's law to orthotropy can be acceptable only when the load intensity is low and not for high strain and for loading direction inclined with respect to the fibre orientation of the material [6].

Many theories on the wood material have been proposed in the literature. Among these, the earliest was that for wood in compression at an inclined angle of fibre, of Hankinson [7], which was extended by Goodman and Bodig [8] to a three dimension. Another model of wood was that of Tsai and Wu [9], which formulated a failure surface expressed as a scalar function of a polynomial tensor. Patton-Mallory et al. [2] used a three-dimensional model of wood, tri-linear elastic-plastic under compression stress and linear elastic, with a tension and shear cut-off, under tension stress.

Tabiei and Wu [10] proposed a continuum FEM model for timber which updated, in an incremental analysis, each component of the elastic moduli of the material stiffness matrix, on the basis of power functions, fitted to test data. This approach did not use any yield function of stress. Schmidt and Kaliske [11] proposed a three-dimensional model which adopted a multi-surface yield approach for elastic-plastic behaviour of wood. Recently, the adoption of FEM numerical codes to analyse the strength of a timber structural member has gained an increasing importance. Often the numerical codes are sophisticated and are specifically capable of

representing the non-linear behaviour of the material [12–15] and some particular effects such as creep [16, 17].

The present work here discusses the following parts: the basic mathematical formulation of the continuum mechanics of solids according to the finite strain theory; the material model for timber: orthotropic, elastic-viscous-plastic, brittle in tension, ductile in compression, based on a multi-surface yield approach; the FEM formulation for large strains and large displacements with 3D solid hexahedral elements, numerical examples, results and discussion.

2. Materials and methods

The FEM is inherently developed according to the theory of the continuum mechanics of solids. In this work a general purpose FEM framework, with three-dimensional hexahedral elements and with a specific material model of wood, has been devised and software coded for the analysis of structural timber, which aims to reproduce the main mechanic performance of a timber element. In this code, the material model has been built in. In compression state, an elastic-viscous-plastic behaviour has been adopted, and in tension an elastic with brittle failure has been adopted. The stress tensor is accounted, at the integration points of an element, to compute the corresponding elastic-viscous-plastic material tangent modulus and the corresponding strain tensor. Failure is computed at a limit value of each component, in compression of both the stress tensor, representing yield, and strain tensor and in tension of the strain tensor only.

2.1. Introduction to the problem of continuum mechanics

According to the classical theory of the continuum mechanics of solids [18–20], the formulation of the FEM for finite strains is based on the description of the deformation state of a generic solid, subjected to a loading condition. The kinematic transformation of a body, from the state at the initial time 0, in the reference configuration ^{O}B, to a successive state at the time t, in the current configuration ^{t}B, is taken under consideration. ^{0}V and ^{t}V are the volumes of the body and ^{0}S and ^{t}S are the boundary surfaces at 0 time and t time, respectively. Displacements $\overline{\mathbf{u}}(\mathbf{x})$, on the portion $^{t}S_{\mathbf{u}}$ and tractions $\overline{\mathbf{t}}(\mathbf{x})$, on the portion $^{t}S_{\mathbf{\sigma}}$ of the solid are specified as boundary conditions. Both body force loads, $\mathbf{b}$, and traction, $\mathbf{t}$, at the surface boundary, are assigned.

The solution to that problem consists to determinate the displacement of a point P, at a time t, of the body from the initial time to the current time, that is:

$$\mathbf{u} = {}^{t}\mathbf{x} - {}^{0}\mathbf{x} \tag{1}$$

where $^{0}\mathbf{x}$ and $^{t}\mathbf{x}$ are the coordinate vectors of the point P at the time 0 and t, respectively.

A basic tensor, which has an important role in the present theory, is the deformation gradient which can be calculated as:

$$\underline{X} = \frac{\partial^t x}{\partial^0 x} \tag{2}$$

The quantities that govern the problem are distinguished if they are referred to the reference configuration, which is known, or to the current configuration, which is instead unknown.

The strains to which the body is subjected can be computed in the reference configuration by the Green-Lagrange strain tensor

$$\underline{E} = \frac{1}{2}(\underline{X}^T \underline{X} - \underline{I}) \tag{3}$$

where $\underline{I}$ is the unit tensor.

The stress tensor is computed through the constitutive law that expresses the stress tensor in terms of the strain tensor, by warranting that the stress and strain measures must be energetically conjugate. Accordingly to this, the Second Piola-Kirchhoff stress tensor, $\underline{S}$, defined in the reference configuration, energetically conjugate to $\underline{E}$, is calculated as:

$$\underline{S} = \det(\underline{X})\underline{X}^{-1}\underline{\sigma} \tag{4}$$

The true stress tensor or Cauchy stress tensor $\underline{\sigma}$, is defined in the current configuration and it is related to $\underline{S}$ as follows:

$$\underline{\sigma} = \frac{1}{\det(\underline{X})}\underline{X}^T\underline{S}\underline{X} \tag{5}$$

The measures of engineering stresses are expressed by the First Piola-Kirchhoff stress tensor, which is computed as

$$\underline{P} = \underline{X}^T\underline{S} \tag{6}$$

The above problem is ruled out by the equation of spatial momentum equilibrium in the reference configuration:

$$^0\rho\ddot{u} = div\,\underline{P} - {}^0\rho\mathbf{b} \tag{7}$$

where $^0\rho$ is the mass density of the body, $\ddot{u}$ is the acceleration, which is set equal to $\ddot{u} = 0$ for the present static case. Also, the momentum equilibrium can be written by the weak form of the virtual work principle in the reference configuration:

$$\int_{^0V} \underline{P} : grad\,\delta\mathbf{v}d^0V - \int_{^0V} {}^0\rho\mathbf{b}\delta\mathbf{v}d^0V - \int_{^0S_\sigma} \bar{t}\delta\mathbf{v}\Gamma d^0S = 0 \tag{8}$$

and in the current configuration:

$$\int_{^tV} \underline{\pmb{\sigma}} : \delta \underline{\mathbf{l}} d^tV - \int_{^tV} {}^t\rho \mathbf{b}\delta \mathbf{v} d^tV - \int_{^tS_\sigma} \bar{t}\delta \mathbf{v} d^tS = 0 \tag{9}$$

where Γ is the inverse Jacobian of surface and

$$\underline{\mathbf{l}} = \frac{\partial \mathbf{v}}{\partial^0 \mathbf{x}}\frac{\partial^0 \mathbf{x}}{\partial^t \mathbf{x}} = \frac{\partial}{\partial t}\left(\frac{\partial^t \mathbf{x}}{\partial^0 \mathbf{x}}\right) : \frac{\partial^0 \mathbf{x}}{\partial^t \mathbf{x}} = \underline{\dot{\mathbf{X}}}\,\underline{\mathbf{X}}^{-1} \tag{10}$$

is the spatial velocity gradient, $\delta \mathbf{v}$ is an admissible virtual velocity and $\delta \underline{\mathbf{l}}$ is the virtual velocity gradient that satisfy $\delta \mathbf{v} = 0$ on both ${}^0S_\mathbf{u}$ and ${}^tS_\mathbf{u}$.

By considering $d^tV = \det(\underline{\mathbf{X}})d^0V$, ${}^t\rho = \det(\underline{\mathbf{X}}){}^0\rho$, $d^tS = \Gamma d^0S$ and the spatial Kirchhoff stress tensor $\underline{\pmb{\tau}} = \det(\underline{\mathbf{X}})\underline{\pmb{\sigma}}$, we obtain the final expression of the principle of virtual work:

$$\int_{^0V} \underline{\pmb{\tau}} : \delta \underline{\mathbf{l}} d^0V - \int_{^0V} {}^0\rho \mathbf{b}\delta \mathbf{v} d^0V - \int_{^0S_\sigma} \bar{t}\delta \mathbf{v}\Gamma d^0S = 0 \tag{11}$$

2.2. Finite element method framework

According to the FEM, the variables in the above equation can be discretized by interpolation forms, h_i and h_j, where $i, j = 1,..n$; n: number of nodes, and the integral equations are linearized to be integrated. The solutions of these non-linear equations can be obtained by the Newton-Raphson iterative method [18–20]. The FEM discretization gives the following system of equations for solving $d\mathbf{u}_j$:

$$\underline{\mathbf{K}}d\mathbf{u}_j + \mathbf{R}_i - \mathbf{F}_i = 0 \quad \forall \{i\} : \mathbf{x}_i \notin S_u \tag{12}$$

$$\mathbf{u}_i = \bar{u}(\mathbf{x}_i) \quad \forall \{i\} : \mathbf{x}_i \in S_u \tag{13}$$

where the nodal force vector is:

$$\mathbf{F}_i = \int_{^0V} {}^0\rho \mathbf{b}h_i d^0V + \int_{^0S_\sigma} \bar{t}h_i \Gamma d^0S \tag{14}$$

the nodal stiffness matrix is:

$$\underline{\underline{\mathbf{K}}} = \int_{^0V} \underline{\underline{\mathbf{D}}}\frac{\partial h_i}{\partial^t \mathbf{x}}\frac{\partial h_j}{\partial^t \mathbf{x}} d^0V - \int_{^0V} \underline{\pmb{\tau}}\frac{\partial h_i}{\partial^t \mathbf{x}}\frac{\partial h_j}{\partial^t \mathbf{x}} d^0V - \int_{^0S_\sigma} \bar{t}h_i \frac{\partial \Gamma}{\partial \mathbf{u}_j} d^0S \tag{15}$$

the nodal residual vector is:

$$\mathbf{R}_i = \int_{^0V} \underline{\pmb{\tau}}\frac{\partial h_i}{\partial^t \mathbf{x}} d^0V \tag{16}$$

and the tangent stiffness matrix is:

$$\underline{\underline{\mathbf{D}}} = \frac{\partial \boldsymbol{\tau}}{\partial \underline{\mathbf{X}}} \underline{\mathbf{X}} \qquad (17)$$

Also, to account that the orthotropic principal axes of the material can rotate with respect to the reference system, the material tensor, constitutive law, must be computed using a rotation tensor $\underline{\mathbf{R}}$ of the orthotropic axes in the reference system, which is determined from the spectral decomposition of the deformation tensor:

$$\underline{\underline{\mathbf{D}}} = \mathbf{R}^{\mathrm{T}} \underline{\underline{\mathbf{D}}}_0 \underline{\mathbf{R}} \qquad (18)$$

where $\underline{\underline{\mathbf{D}}}_0$ is the material tensor and $\underline{\underline{\mathbf{D}}}$ is the same material tensor rotated in the reference system.

The tangent stiffness matrix in general is non-symmetric and is dependent on the material tangent modulus. Its computation requires an adequate numerical approach which has to be generally relied to the constitutive relationships of the specific material.

The above non-linear system of Eqs. (12) and (13), at a global level, by applying the Newton-Raphson Method, is iteratively solved with the trial solution $\mathbf{u}_i$, updated with $d\mathbf{u}_j$. Coherently to solve the updated system, the above equations, the stiffness matrix, the residual vector and the force vector are updated. The convergence of the solution is checked on a measure of error, the root mean square of the $d\mathbf{u}_j$ or the nodal residual vector, the un-equilibrated force $-\mathbf{R}_i + \mathbf{F}_i$.

2.3. The constitutive material model

The non-linear behaviour of a material can be analysed by constitutive equations which relate stress to strain and other internal variables in a rate form. Within the finite strain hypothesis, constitutive equations must be formulated by warranting the principle of objectivity, that is, they must remain indifferent to the change of reference frame. This can be guaranteed by utilizing the objective tensor in constitutive equations.

In recent scientific literature some authors have proposed numerical solutions to the problem of continuum and consistent elastic-viscous-plasticity. Many scientific papers have been developed within the hypothesis of small strains [21–26], and others have focused their attention on finite strains hypothesis [27–31]. Many theoretical and numerical methods have been proposed in the literature to perform the procedure of stress update, in an incremental objectivity. The formulation of an incremental objective algorithm is based on constitutive equations, expressed as objective spatial rate, which are mapped to an intermediate configuration (in the present paper the relative variables are denoted with '^'). This configuration is a fictitious configuration which remains indifferent to rigid rotation. Also, the principle of objectivity is guaranteed by appropriate tensorial transformation of the body between spatial and material configuration.

Coherently to the above assertions, in the present work a convective or material representation [32, 33] has been employed. The problem is analysed by adopting the well-known multiplicative

elasto-plasticity theory [32, 34] which postulates the multiplicative decomposition of the deformation gradient in an elastic part $\underline{\mathbf{X}}_e$ and a plastic (in the present work, the term 'plastic' means 'inelastic' in a more wide sense) part $\underline{\mathbf{X}}_p$:

$$\underline{\mathbf{X}} = \underline{\mathbf{X}}_e \underline{\mathbf{X}}_p \tag{19}$$

From the above discussion, the intermediate configuration can be described by the plastic part of the deformation gradient, $\underline{\mathbf{X}}_p$, except for a rigid rotation.

In order to formulate the elastic-viscous-plastic kinematics, a consistent transformation to the intermediate configuration is introduced for the spatial velocity gradient:

$$\underline{\mathbf{l}} = \dot{\underline{\mathbf{X}}} \, \underline{\mathbf{X}}^{-1} = \underline{\mathbf{l}}_e + \underline{\mathbf{l}}_p \tag{20}$$

where $\underline{\mathbf{l}}_e$ is the elastic part of the spatial velocity gradient and $\underline{\mathbf{l}}_p$ is the plastic part of the spatial velocity gradient.

The material velocity gradient is:

$$\underline{L} = \underline{\mathbf{X}}_e^{-1} \underline{\mathbf{l}} \underline{\mathbf{X}}_e = \underline{L}_e + \underline{L}_p \tag{21}$$

By mapping $\underline{\mathbf{l}}_e$ and $\underline{\mathbf{l}}_p$ to the intermediate configuration we obtain

$$\hat{\underline{L}}_e = \underline{\mathbf{X}}_e^{-1} \dot{\underline{\mathbf{X}}}_e \text{ the elastic part} \tag{22}$$

and

$$\hat{\underline{L}}_p = \dot{\underline{\mathbf{X}}}_p \underline{\mathbf{X}}_p^{-1} \text{ the plastic part} \tag{23}$$

of the velocity gradient $\hat{L}$ in the intermediate configuration.

The stress power per unit reference volume is:

$$\mathcal{P} = \underline{\Sigma} : \hat{\underline{L}} \tag{24}$$

where the stress measure, work-conjugate to $\hat{\underline{L}}$, is the Mandel stress tensor $\underline{\Sigma} = \underline{\mathbf{C}}_e \hat{\underline{S}}$, generally non-symmetric, $\underline{\mathbf{C}}_e = \underline{\mathbf{X}}_e^{\mathbf{T}} \underline{\mathbf{X}}_e$ is the elastic Cauchy-Green tensor, and $\hat{\underline{S}} = \underline{\mathbf{X}}_p \underline{\mathbf{S}} \underline{\mathbf{X}}_p^{\mathbf{T}}$ is the Second Piola-Kirchhoff stress tensor in the intermediate configuration.

The constitutive relationships must conform to some restrictions [35], which derive from the second law of thermodynamics, expressed as the Clausius-Planck inequality. By considering an isothermal process and a purely mechanical case, the above inequality is expressed as plastic dissipation per unit reference volume:

$$D = \frac{1}{2}\hat{\underline{S}} : \dot{\hat{\underline{C}}}_e - \dot{\hat{\Psi}} \geq 0 \qquad (25)$$

where

D is the dissipation; $\hat{\Psi} = \hat{\Psi}(\hat{\underline{C}}_e, \hat{\chi})$ is the free energy function, expressed in terms of $\hat{\underline{C}}_e$, and the internal variables $\hat{\chi}$ conjugate to the internal stresses $\hat{q}$.

The material time derivative of the free energy is

$$\dot{\hat{\Psi}} = \frac{\partial\hat{\Psi}}{\partial\hat{\underline{C}}_e} : \dot{\hat{\underline{C}}}_e + \frac{\partial\hat{\Psi}}{\partial\hat{\chi}} \cdot \dot{\hat{\chi}} \qquad (26)$$

and the inequality results as:

$$D = \left(\hat{\underline{S}} - 2\frac{\partial\hat{\Psi}}{\partial\hat{\underline{C}}_e}\right) : \dot{\hat{\underline{C}}}_e + \underline{\Sigma} : \hat{\underline{L}}_p - \frac{\partial\hat{\Psi}}{\partial\hat{\chi}}\dot{\hat{\chi}} \geq 0 \qquad (27)$$

The inequality (25) being valid for any admissible process of the material and from Eqs. (26) and (27) the constitutive equations are obtained as:

$$\hat{\underline{S}} = 2\frac{\partial\hat{\Psi}}{\partial\hat{\underline{C}}_e} \qquad (28)$$

and

$$\hat{q} = \frac{\partial\hat{\Psi}}{\partial\hat{\chi}} \qquad (29)$$

where $\hat{q}$ is the internal stress vector conjugate to the internal variables $\hat{\chi}$.

Hence the reduced dissipation inequality in a local form is:

$$D = \underline{\Sigma} : \hat{\underline{L}}_p - \hat{q} \cdot \dot{\hat{\chi}} \geq 0 \qquad (30)$$

The hardening or softening law is expressed as follows:

$$\dot{\hat{\chi}} = \sum_m \dot{\gamma}_m \mathbf{H}_m(\hat{\underline{S}}, \hat{q}) \qquad (31)$$

where γ_m are the plastic multipliers, $m = 1, \ldots, s$ and s is the number of multi-surfaces of yield, and $\mathbf{H}_m$ is the hardening or softening modulus, these quantities in the case of isotropic hardening or softening are scalars.

In the case of elastic response of stress, the response can be formulated in a non-rate form with a hyper-elastic potential in the intermediate configuration $\hat{\Psi}(\hat{\underline{C}}_e)$, this statement satisfy directly the principle of objectivity [28]. Thus

$$\hat{\Psi}(\underline{\hat{C}}_e) = \frac{1}{2}\underline{\hat{S}} : \underline{\hat{\dot{C}}}_e \tag{32}$$

and [36]

$$\underline{\hat{S}} = 2\frac{\partial\hat{\Psi}}{\partial\underline{\hat{C}}_e} \tag{33}$$

is the Second Piola-Kirchhoff stress tensor in the intermediate configuration. From the differential of Eq. (32), the fourth-order elastic modulus tensor in the intermediate configuration can be obtained as:

$$\underline{\underline{\hat{D}}}_e = 2\frac{\partial\underline{\hat{S}}}{\partial\underline{\hat{C}}_e} = 4\frac{\partial^2\hat{\Psi}}{\partial\underline{\hat{C}}_e\partial\underline{\hat{C}}_e} \tag{34}$$

In the case of rate-independent elastic-plasticity, without the viscous effect, the point representative of stress cannot come outside the yield surfaces, identified by the yield functions $\hat{f}_m(\underline{\hat{S}},\hat{q})$.

Note that in the following expression the stresses $\underline{\hat{S}}$ include the back stresses $-\hat{\beta}$. The plastic multiplier γ_m can be computed by forcing the optimization conditions, named the Kuhn-Tucker loading/unloading conditions:

$$\dot{\gamma}_m \geq 0, \ \hat{f}_m \leq 0, \ \dot{\gamma}_m\hat{f}_m = 0 \tag{35}$$

and the consistency conditions:

$$\dot{\gamma}_m\hat{\dot{f}}_m = 0 \tag{36}$$

In the case of rate-dependent visco-plasticity, the actual stress can overcome out the yield surface, and consequently the above condition is no longer appropriate, but an overstress function $\hat{\Phi}_m(\underline{\hat{S}},\hat{q})$ of the yield criteria can be defined such that:

$$\hat{\Phi}_m = 0 \ when \ \hat{f}_m \leq 0 \ and \ \hat{\Phi}_m = \hat{f}_m \ when \ \hat{f}_m > 0 \tag{37}$$

The viscous-plastic flow is evaluated by the following relaxation equation

$$\dot{\gamma}_m = \frac{1}{\eta}\hat{\Phi}_m \tag{38}$$

whose discretized form is:

$$\Delta\gamma_m = \frac{\Delta t_{t+\Delta t}}{\eta}\hat{\Phi}_m \tag{39}$$

where $\eta = 1$ is a viscosity parameter and $\eta \to 0$ in case of no viscid effects.

In order to determine the plastic stress response in Eq. (30), the plastic dissipation requires to compute the plastic part of the deformation gradient. From the principle of maximum plastic dissipation, the evolution equations of the inelastic strain tensors can be determined as normality rules:

$$\hat{\underline{L}}_p = \sum_m \dot{\gamma}_m \frac{\partial \hat{\Phi}_m}{\partial \underline{\Sigma}} \tag{40}$$

$$\hat{\chi} = \sum_m \dot{\gamma}_m \frac{\partial \hat{\Phi}_m}{\partial \hat{q}} \tag{41}$$

The introduction of the consistency multipliers allows to distinguish the different material response upon each yield surface as follows:

$$\gamma_m = 0 \Rightarrow elastic\ response$$

$$\gamma_m > 0 \Rightarrow plastic\ response.$$

2.4. Objective integration algorithm

The constitutive equations can be approximately solved at a local level, with a general return mapping procedure. The time integration has been executed with a backward Euler scheme fully implicit in time, and an exponential map has been adopted for the plastic deformation gradient. According to this scheme of time integration, from a given state at the previous time step t, characterized by $^t\underline{X}$ and $^t\underline{X}_p$ and using the displacement increment $\Delta\mathbf{u}$, the deformation gradient $^{t+\Delta t}\underline{X}$ can be determined. The trial elastic strain tensor $\hat{\underline{E}}^{trial}$ can be computed from the plastic deformation gradient $^t\underline{X}_p$ in the previous time step t.

The multiplicative decomposition, Eq. (19) is discretized

$$^{t+\Delta t}\underline{X} = {}^{t+\Delta t}\underline{X}_e{}^{t+\Delta t}\underline{X}_p \tag{42}$$

From the Eqs. (23) and (40) $\hat{\underline{L}}_p$ the flow rule can be recast in the following form:

$$\hat{\underline{L}}_p = \dot{\underline{X}}_p \underline{X}_p^{-1} = \sum_m \dot{\gamma}_m \hat{\underline{N}}_m \tag{43}$$

where

$$\hat{\underline{N}}_m = \frac{\partial \hat{\Phi}_m}{\partial \underline{\Sigma}} \tag{44}$$

is the viscous-plastic flow direction where the plastic potential coincide with the yield function, in an associative visco-plasticity.

The hardening or softening law has been discretized as follows:

$$^{t+\Delta t}\hat{\chi} = {}^{t}\hat{\chi} + \sum_{m} \Delta\gamma_m{}^{t+\Delta t}\mathbf{H}_m(\underline{\hat{S}}, \hat{q}) \tag{45}$$

From the above Eq. (43), it is possible to obtain:

$$\underline{\dot{\mathbf{X}}}_p = \sum_{m} \dot{\gamma}_m \underline{\hat{N}}_m \underline{\mathbf{X}}_p \tag{46}$$

the same relation can be integrated in time by an implicit backward Euler procedure, from t to $t + \Delta t$, with a time increment Δt and with an exponential shift [28]:

$$^{t+\Delta t}\underline{\mathbf{X}}_p = \exp\left(\sum_{m} \Delta\gamma_m{}^{t+\Delta t}\underline{\hat{N}}_m\right){}^{t}\underline{\mathbf{X}}_p \cong \left(\underline{\mathbf{I}} + \sum_{m} \Delta\gamma_m{}^{t+\Delta t}\underline{\hat{N}}_m\right){}^{t}\underline{\mathbf{X}}_p \tag{47}$$

where $\Delta\gamma_m = \Delta t \dot{\gamma}_m$ is the step increment of the consistent elastic-viscous-plastic multiplier. In the above discretization the direction of the plastic flow has been taken constant throughout the increment and is equal to its final value $^{t+\Delta t}\underline{\hat{N}}_m$ which is assumed to be equal to that of the trial step.

Then the continuum elastic-viscous-plastic tangent stiffness matrix, which expresses the derivative of stress to respect to strain, it can be determined:

$$\underline{\hat{\mathbf{D}}} = \left[\underline{\hat{\mathbf{D}}}_e - \frac{\left(\underline{\hat{\mathbf{D}}}_e : \sum_{m} \hat{\mathbf{N}}_m\right) \otimes \left(\underline{\hat{\mathbf{D}}}_e : \sum_{m} \hat{\mathbf{N}}_m\right)}{\left(\sum_{m} \hat{\mathbf{N}}_m : \underline{\hat{\mathbf{D}}}_e : \sum_{m} \hat{\mathbf{N}}_m - \sum_{m} \frac{\partial\hat{\Phi}_m}{\partial\hat{q}} \cdot \mathbf{H}_m + \eta \cdot c_{creep}\right)}\right] \tag{48}$$

where the creep term is expressed as follows:

$$c_{creep} = \left(\frac{1}{a_1 \sum_{m} \Delta\gamma_m}\right) \left(\frac{\sum_{m} \Delta\gamma_m}{\Delta t \dot{\bar{\varepsilon}}_{c0} t^{a_2}}\right)^{\frac{1}{a_1}} \tag{49}$$

where the power law for creep is evaluated [16] as:

$$\bar{\varepsilon}_c = \Delta t a_0 \bar{\sigma}^{a_1} t^{a_2} \tag{50}$$

where

$\bar{\varepsilon}_c$ is the uniaxial creep strain;

$\dot{\bar{\varepsilon}}_{c0}$ is a reference creep strain rate; $\bar{\sigma}$ is the equivalent stress; a_0 is the coefficient in the creep power law, which is strain rate; a_1: is the exponent of the equivalent stress in creep power law; a_2 is the exponent of time in creep power law; Δt: is the time increment.

The trial stress predictor is computed as

$$\underline{\hat{S}}^{trial} = \underline{\hat{D}}_e : \underline{\hat{E}}^{trial} \tag{51}$$

and in discretized form

$$^{t+\Delta t}\underline{\hat{S}} = \underline{\hat{D}}_e : {}^{t+\Delta t}\underline{\hat{E}}^{trial} \tag{52}$$

where

$$\underline{\hat{E}}^{trial} = \frac{1}{2}({}^{t+\Delta t}\underline{X}^{T\,t+\Delta t}\underline{X} - I) \tag{53}$$

Substituting the Eqs. (42) and (47) into the elastic Green Lagrange strain tensor, we have:

$$\underline{\hat{E}} = \underline{X}_p^{T-1}\underline{\hat{E}}^{trial}\underline{X}_p^{-1} \tag{54}$$

For all the multi-surface yields, by using the proper yield criterion, the trial overstress function $\hat{\Phi}_m^{trial}$ can be computed and hence the flow direction $\underline{\hat{N}}_m^{trial}$ can be evaluated as norm of the deviatoric stress tensor $\| DEV(\underline{\hat{S}}^{trial}) \|$. In the case of elastic response, the values of the variables at current time $t + \Delta t$ are equal to their respective predictors. Instead, in the case of plastic response by using the exponential mapping (47), the stress point is mapped back to the yield surface.

Then, the increment of each plastic multiplier $\Delta\Delta\gamma_m$, discretized in time, in the case of plastic loading $^{t+\Delta t}\hat{\Phi}_m = 0$, can be solved for each $^{t+\Delta t}\Delta\gamma_m$ by means of a local iterative Newton-Rapshon Method.

For all the multi-surfaces, at the end of each local iteration, the intermediate configuration, described by $^{t+\Delta t}\underline{X}_p$ and the internal variables are updated.

The updated stress tensor is evaluated as follows:

$$\underline{\hat{S}} = \underline{\hat{D}} : \underline{\hat{E}} - \sum_m \Delta\gamma_m\underline{\hat{N}}_m \tag{55}$$

In the following expressions

$$^{t+\Delta t}\underline{\hat{E}}_p = {}^t\underline{\hat{E}}_p + {}^{t+\Delta t}\Delta\underline{\hat{E}}_p \tag{56}$$

$$^{t+\Delta t}\hat{\chi} = {}^t\hat{\chi} + {}^{t+\Delta t}\Delta\hat{\chi} \tag{57}$$

the increments are evaluated as follows:

$$^{t+\Delta t}\Delta\hat{\underline{E}}_p = \sum_m {}^{t+\Delta t}\Delta\gamma_m \frac{\partial^{t+\Delta t}\hat{\Phi}_m}{\partial\hat{\underline{S}}} \tag{58}$$

$$^{t+\Delta t}\Delta\hat{\chi} = -\sum_m {}^{t+\Delta t}\Delta\gamma_m \frac{\partial^{t+\Delta t}\hat{\Phi}_m}{\partial\hat{q}} \tag{59}$$

by introducing the residual vectors:

$$^{t+\Delta t}\mathbf{r}_p = -^{t+\Delta t}\hat{\underline{E}}_p + {}^t\hat{\underline{E}}_p + {}^{t+\Delta t}\Delta\hat{\underline{E}}_p = 0 \tag{60}$$

$$^{t+\Delta t}\mathbf{r}_\chi = {}^{t+\Delta t}\hat{\chi} - {}^t\hat{\chi} - {}^{t+\Delta t}\Delta\hat{\chi} = 0 \tag{61}$$

$$^{t+\Delta t}r_\Phi = {}^{t+\Delta t}\hat{\Phi}_m\left({}^{t+\Delta t}\hat{\underline{S}}, {}^{t+\Delta t}\hat{q}\right) = 0 \tag{62}$$

which are solved for the variables:

$$\left\{ \begin{array}{c} ^{t+\Delta t}\hat{\underline{S}} \\ ^{t+\Delta t}\hat{q} \\ ^{t+\Delta t}\Delta\gamma_m \end{array} \right\} \tag{63}$$

By linearizing [37] the residual vectors, a system of linear equations is obtained:

$$^{t+\Delta t}\mathbf{r}_p + \frac{\partial^{t+\Delta t}\mathbf{r}_p}{\partial\hat{\underline{S}}} : \Delta\hat{\underline{S}} + \frac{\partial^{t+\Delta t}\mathbf{r}_p}{\partial\hat{q}} : \Delta\hat{q} + \frac{\partial^{t+\Delta t}\mathbf{r}_p}{\partial\Delta\gamma_m} : \Delta\Delta\gamma_m = 0 \tag{64}$$

$$^{t+\Delta t}\mathbf{r}_\chi + \frac{\partial^{t+\Delta t}\mathbf{r}_\chi}{\partial\hat{\underline{S}}} : \Delta\hat{\underline{S}} + \frac{\partial^{t+\Delta t}\mathbf{r}_\chi}{\partial\hat{q}} : \Delta\hat{q} + \frac{\partial^{t+\Delta t}\mathbf{r}_\chi}{\partial\Delta\gamma_m} : \Delta\Delta\gamma_m = 0 \tag{65}$$

$$^{t+\Delta t}r_\Phi + \frac{\partial^{t+\Delta t}r_\Phi}{\partial\hat{\underline{S}}} : \Delta\hat{\underline{S}} + \frac{\partial^{t+\Delta t}r_\Phi}{\partial\hat{q}} : \Delta\hat{q} + \frac{\partial^{t+\Delta t}r_\Phi}{\partial\Delta\gamma_m} : \Delta\Delta\gamma_m = 0 \tag{66}$$

Dropping the superscript $t + \Delta t$ and writing:

$$\underline{\underline{\Xi}}^{-1} = \underline{\underline{\hat{D}}}_e^{-1} + \Delta\gamma_m \frac{\partial^2\hat{\Phi}_m}{\partial\hat{\underline{S}}\partial\hat{\underline{S}}} \tag{67}$$

and

$$\underline{\underline{\Omega}}^{-1} = \underline{\underline{\mathbf{H}}}^{-1} + \Delta\gamma_m \frac{\partial^2\hat{\Phi}_m}{\partial\hat{q}\partial\hat{q}} \tag{68}$$

the solution can be obtained as

$$\begin{bmatrix} {}^{t+\Delta t}\Delta\underline{\hat{S}} \\ {}^{t+\Delta t}\Delta\underline{\hat{q}} \\ {}^{t+\Delta t}\Delta\Delta\gamma_m \end{bmatrix} = \begin{bmatrix} \underline{\underline{\Xi}}^{-1} & \Delta\gamma_m\dfrac{\partial^2\hat{\Phi}_m}{\partial\hat{q}\partial\underline{\hat{S}}} & \dfrac{\partial\hat{\Phi}_m}{\partial\underline{\hat{S}}} \\ \Delta\gamma_m\dfrac{\partial^2\hat{\Phi}_m}{\partial\underline{\hat{S}}\partial\hat{q}} & \underline{\underline{\Omega}}^{-1} & \dfrac{\partial\hat{\Phi}_m}{\partial\hat{q}} \\ \dfrac{\partial\hat{\Phi}_m}{\partial\underline{\hat{S}}} & \dfrac{\partial\hat{\Phi}_m}{\partial\hat{q}} & 0 \end{bmatrix}^{-1} \cdot \begin{bmatrix} -\mathbf{r}_p \\ -\mathbf{r}_\chi \\ -r_\Phi \end{bmatrix} \tag{69}$$

where the consistent Jacobian, $\mathbf{J}$, of the residuals is:

$$\frac{d\mathbf{r}}{d\mathbf{z}} = \mathbf{J}^{-1} = \begin{bmatrix} \underline{\underline{\Xi}}^{-1} & \Delta\gamma_m\dfrac{\partial^2\hat{\Phi}_m}{\partial\hat{q}\partial\underline{\hat{S}}} & \dfrac{\partial\hat{\Phi}_m}{\partial\underline{\hat{S}}} \\ \Delta\gamma_m\dfrac{\partial^2\hat{\Phi}_m}{\partial\underline{\hat{S}}\partial\hat{q}} & \underline{\underline{\Omega}}^{-1} & \dfrac{\partial\hat{\Phi}_m}{\partial\hat{q}} \\ \dfrac{\partial\hat{\Phi}_m}{\partial\underline{\hat{S}}} & \dfrac{\partial\hat{\Phi}_m}{\partial\hat{q}} & 0 \end{bmatrix}^{-1} \tag{70}$$

the vector of unknowns is:

$$\mathbf{z} = \begin{bmatrix} {}^{t+\Delta t}\Delta\underline{\hat{S}} \\ {}^{t+\Delta t}\Delta\underline{\hat{q}} \\ {}^{t+\Delta t}\Delta\Delta\gamma_m \end{bmatrix} \tag{71}$$

and the vector of residual is:

$$\mathbf{r} = \begin{Bmatrix} \mathbf{r}_p \\ \mathbf{r}_\chi \\ r_\Phi \end{Bmatrix} \tag{72}$$

The system of equations is solved by the Newton-Raphson following iteration scheme:

$$\mathbf{z}_{k+1} = \mathbf{z}_k - \mathbf{J}^{-1}\mathbf{r}_k \tag{73}$$

where k is the iteration number. However, in a more advantageous mode the system of equations has been solved by partitioning Eq. (69) into submatrices.

At the start of the iteration loop the following positions are made:

$$^{t+\Delta t}\underline{\hat{E}}_p^{(0)} = {}^t\underline{\hat{E}}_p \tag{74}$$

$$^{t+\Delta t}\underline{\hat{\chi}}^{(0)} = {}^t\underline{\hat{\chi}} \tag{75}$$

$$^{t+\Delta t}\Delta\gamma_m^{(0)} = {}^t\Delta\gamma_m \tag{76}$$

At each iteration k the following quantities are computed:

$$^{t+\Delta t}\Delta\hat{\underline{E}}_p^{(k)} = -\hat{\underline{\underline{D}}}_e^{-1\,t+\Delta t}\Delta\hat{\underline{S}} \tag{77}$$

$$^{t+\Delta t}\Delta\hat{\chi}^{(k)} = \underline{\underline{H}}^{-1\,t+\Delta t}\Delta\hat{q} \tag{78}$$

$$^{t+\Delta t}\Delta\gamma_m^{(k)} = {}^{t+\Delta t}\Delta\gamma_m \tag{79}$$

hence the internal variables are updated as follows:

$$^{t+\Delta t}\hat{\underline{E}}_p^{(k+1)} = {}^{t+\Delta t}\hat{\underline{E}}_p^{(k)} + {}^{t+\Delta t}\Delta\ddot{\underline{E}}_p^{(k)} \tag{80}$$

$$^{t+\Delta t}\hat{\chi}^{(k+1)} = {}^{t+\Delta t}\hat{\chi}^{(k)} + {}^{t+\Delta t}\Delta\hat{\chi}^{(k)} \tag{81}$$

$$^{t+\Delta t}\Delta\gamma_m^{(k+1)} = {}^{t+\Delta t}\Delta\gamma_m^{(k)} + {}^{t+\Delta t}\Delta\Delta\gamma_m^{(k)} \tag{82}$$

The next step begins by computing the stress tensor and the internal stress tensor. The iterations progress until the norm of the residual vectors stays behind a prefixed tolerance.

At this point each overstress function can be defined as follows:

$$\hat{\Phi}_m(\hat{\underline{S}}, \hat{q}) = |DEV(\hat{S}_{ij}) + \hat{q}_{ij}| - \frac{3}{2}s_{mat} - s_{flow} \tag{83}$$

where:

i, j are the indexes which define the nine components of the stress and strain tensors; DEV is the deviatoric operator; $s_{mat} = [\hat{\underline{N}}_m \cdot (\underline{\underline{\Xi}} : \hat{\underline{N}}_m) + \hat{\underline{N}}_m \cdot (\underline{\underline{\Omega}} : \hat{\underline{N}}_m)]\Delta\gamma_m + [\mathbf{r} \cdot (\underline{\underline{\Xi}} : \hat{\underline{N}}_m) + \mathbf{r} \cdot (\underline{\underline{\Omega}} : \hat{\underline{N}}_m)]$; $s_{flow} = Y_m\left(1 + \frac{\overline{\varepsilon}_p + \Delta\overline{\varepsilon}_p}{\overline{\varepsilon}_0}\right) \cdot \left(\frac{\Delta\overline{\varepsilon}_p}{\Delta t \cdot \dot{\overline{\varepsilon}}_{c0} t^{a_2}}\right)^{\frac{1}{a_1}}$ is the stress flow due to creep effects; $s_{flow} = Y_m\left(1 + \frac{\overline{\varepsilon}_p + \Delta\overline{\varepsilon}_p}{\overline{\varepsilon}_0}\right)$ is the stress flow without creep effects; $\overline{\varepsilon}_p$ is the equivalent accumulated plastic strain; $\Delta\overline{\varepsilon}_p$ is the increment of the equivalent plastic strain; $\overline{\varepsilon}_0$ is a reference strain assumed as the strain correspondent to Y_m; $\dot{\overline{\varepsilon}}_{c0}$ is a reference creep strain rate; m are multi-surface indexes; $\hat{S}_{ij}$ are the components of the stress tensor $\hat{\underline{S}}$; $\hat{q}_{ij}$ are the components of the hardening tensor $\hat{q}$; Y_m is the initial yield value of the $m-th$ yield surface which is assumed as follows

$$Y_m = \begin{cases} Y_{ij}^t & if\ \hat{S}_{ij} \geq 0 \\ Y_{ij}^c & if\ \hat{S}_{ij} < 0 \end{cases} for\ i, j = 1, ..., 3 \tag{84}$$

Y_{ij}^t are tensile values and Y_{ij}^c are compressive values, nine components which reduce to six for symmetry. The initial yield values are material parameters, which can be identified by experimental tests.

To enhance the convergence in the equilibrium iteration, with the Newton-Raphson Method, the consistent elastic-viscous-plastic tangent stiffness matrix can be used instead of the continuum elastic-viscous-plastic tangent stiffness matrix (48). This is the consequence of the discretization of the consistency condition in correspondence of the rate-independent elastic limit. It can be

obtained by substituting the matrix $\underline{\underline{\hat{D}}}_e$, in the expression (48) the following pseudoelastic material stiffness matrix:

$$\underline{\underline{P}} = \underline{\underline{\hat{D}}}_e^{-1} + \sum_m \Delta\gamma_m \frac{\partial^2 \hat{\Phi}_m}{\partial\underline{\hat{S}}\partial\underline{\hat{S}}} \tag{85}$$

2.5. The finite element method implementation

The previous non-linear constitutive material model has been implemented in a three-dimensional finite element code, based on the displacement approach. The geometry was schematized by adopting linear hexahedral solid iso-parametric elements with eight node. The spatial integration was carried out for each element with an 8-point Gauss quadrature rule.

Within the framework of the Newton-Raphson iteration method, the solution of the non-linear equilibrium equation system was found for the displacements as unknown variables.

The procedure implemented in the software code is listed in **Table 1**.

---

1. Read input file with the following data:
   a. Material constants
   b. Failure constants
   c. Point coordinates of finite elements
   d. Volume vertex points
   e. Groups of element materials
   f. Boundary points restrained
   g. Time-load increment functions
   h. Time steps at each time-load increment
   i. Force-loads
   j. Mass-proportional loads
   k. Volume element subject to mass-proportional loads
   l. Points subject to force-loads
2. Apply the load increment at a prescribed time-step
3. Solve the system of non-linear equations applying the Newton-Raphson Method (NRM) at a global level:
   a. While (Error>tolerance) and (Residue>tolerance) do
   b. Begin
   c. Execute an internal NRM loop for the elastic-viscous-plastic elements
   d. Compute the element stiffness and assemble the global stiffness matrix
   e. Compute the element force and assemble the global force vector
   f. Compute the global residual vector
   g. Update the global correction

---

    h.   Update the restrains

    i.   Update the assigned displacements

    j.   Solve the system of equations

    k.   Update the global displacements

    l.   Compute displacement Error and force Residue for check convergence

    m.   Check against the convergence criteria. The procedure goes to step 3 when the convergence is not reached, and solve the global system of non-linear equations on the vector of residual forces. On the contrary, the procedure progress to a successive time-step, go to step 2 by applying a load increment, when the convergence is reached.

    n.   End of loop

4.   Update the global state, stress tensor, strain tensor and accumulated plastic strain

5.   Update the total displacement vector

6.   Update the geometrical nonlinearity

7.   Output the results, displacements, stresses, strains and accumulated plastic strain.

Table 1. Scheme of the implementation of the software code.

The FEM code was employed to simulate the load-displacement behaviour of white spruce timber up to and beyond failure. Simple tests in tension and in compression have been run to check the ability of the computational code.

2.6. Comparison with experimental data and numerical example

As a check to the suggested implementation, application examples by using the present model have been simulated with the software code. The hexahedron 3D solid elements have been used to mesh timber. Note that the purpose of these tests is to make a preliminary check of the proposed model. Subsequently, the improvement of this model and of its parameters, and further checks against experimental data, is a future task.

To verify the present model preliminarily, a comparison between numerical results and experimental data has been reported here. The experimental data concern a test on a specimen of white spruce under compressive loading, with the loading axes set along the longitudinal fibre of wood. The specimen has been dimensioned with size 20 mm × 20 mm × 20 mm. The experimental data have been assumed from a previous work [6]. In this work, the specimen has been tested by an electro-mechanical press, whose computer controlled the displacement rate at 8 mm/min. The specimen has been loaded until it failed. In this test the elastic and post-elastic stress-strain path of the material has been data-logged. The numerical results have been obtained by referring to the dimensions and mechanical characteristics of the same specimen in order to reproduce the test on the real specimen effectively. The mechanical characteristics of the white spruce wood, assumed from Refs. [6, 38] in the present work, are reported in **Tables 2** and **3**. However, in this numerical test not any fracture has been considered, by reducing the compressive maximum strains respect to those measured in [6]. The creep parameters assumed from [16] are reported in **Table 4**. The simulation of the non-linear behaviour of a wood specimen under compression test has been executed by using a finite element mesh of eight node hexahedral elements, with 1000

elements and 1331 nodes. The specimen has been cinematically restrained at its bottom surface edge, whereas it has been subjected to an impressed displacement path at its top surface edge. The loading simulation has been carried out in control of displacement.

Property	E_{11}	G_{12}	G_{13}	G_{21}	E_{22}	G_{23}	G_{31}	G_{32}	E_{33}
	N/mm^2	N/mm^2	N/mm^2	N/mm^2	N/mm^2	N/mm^2	N/mm^2	N/mm^2	N/mm^2
Elastic modulus [6]	557	38	790	(1)	1010	829	(1)	(1)	12961
	ν_{12}	ν_{13}	ν_{21}		ν_{23}	ν_{31}	ν_{32}		
Poisson's ratio [38]	0.435	0.467	(2)		0.372	(2)	(2)		

(1) To satisfy the objectivity condition, the shear moduli, according to Lekhnitskii [39] are assumed as: $G_{ij} = \frac{E_{ii}E_{jj}}{E_{ii}(1+v_{ij})+E_{jj}(1+v_{ji})}$.

(2) The Poisson's ratios are taken as constant, and to satisfy the symmetry of the elasticity tensor, obeying the relations: $\frac{v_{ij}}{E_{ii}} = \frac{v_{ji}}{E_{jj}}$.

Table 2. Mechanical properties assumed for spruce wood in the numerical tests (E is the elastic modulus, G is the shear modulus and ν is the Poisson ratio, i, j = 1, 2, 3 are the indices, which correspond to longitudinal, radial and tangential fibre directions, respectively).

	Y^t_{11}	Y^t_{12}	Y^t_{13}	Y^t_{21}	Y^t_{22}	Y^t_{23}	Y^t_{31}	Y^t_{32}	Y^t_{33}
	N/mm^2	N/mm^2	N/mm^2	N/mm^2	N/mm^2	N/mm^2	N/mm^2	N/mm^2	N/mm^2
Tensile strength (numerical)	4.0	6.0	6.0	6.0	4.0	6.0	6.0	6.0	40.0
	Y^c_{11}	Y^c_{12}	Y^c_{13}	Y^c_{21}	Y^c_{22}	Y^c_{23}	Y^c_{31}	Y^c_{32}	Y^c_{33}
	N/mm^2	N/mm^2	N/mm^2	N/mm^2	N/mm^2	N/mm^2	N/mm^2	N/mm^2	N/mm^2
Compressive strength [6]	4.0	6.0	6.0	6.0	4.0	6.0	6.0	6.0	40.0
	ε^c_{11}	ε^c_{12}	ε^c_{13}	ε^c_{21}	ε^c_{22}	ε^c_{23}	ε^c_{31}	ε^c_{32}	ε^c_{33}
	adim.	adim.	adim.	adim.	adim.	adim.	adim.	adim.	adim.
Compressive maximum strain (numerical)	0.005	0.005	0.005	0.005	0.005	0.005	0.005	0.005	0.005

Table 3. Strength properties assumed for spruce wood in the numerical tests, which are named as tensile values Y^t_{ij} or compressive values Y^c_{ij}, i, j = 1, 2, 3 are the indices that correspond to longitudinal, radial and tangential fibre directions, respectively.

$\dot{\bar{\varepsilon}}_{c0}$	a_1	a_2
adim.	adim.	adim.
1.0627E-7	4.7290	0.1458

Table 4. Creep parameters assumed for spruce wood in the numerical tests.

Another simulation has been reported as an example. It consists of the reproduction of the non-linear behaviour of a wood specimen under tension loading. The wood specimen has been dimensioned with a size of 20 mm × 10 mm × 240 mm, assuming that the orientation of the longitudinal fibre of wood is set along the loading axes. The simulation has been executed by using a finite element mesh of eight node hexahedral elements with 700 elements and 1188 nodes. In the test, the specimen has been restrained at its bottom surface edge and it has been subjected to an imposed displacement course at its top surface edge. The loading simulation has been carried out in control of displacement.

3. Results and discussion

The stress-strain data of both the experimental and numerical results for the specimen under compression loading have been plotted in **Figure 1**. One can view that the mechanical behaviour is properly predicted both for the elastic tract and for the yielding zone, although the last part of the elastic path, numerically predicted, stays slightly behind that measured.
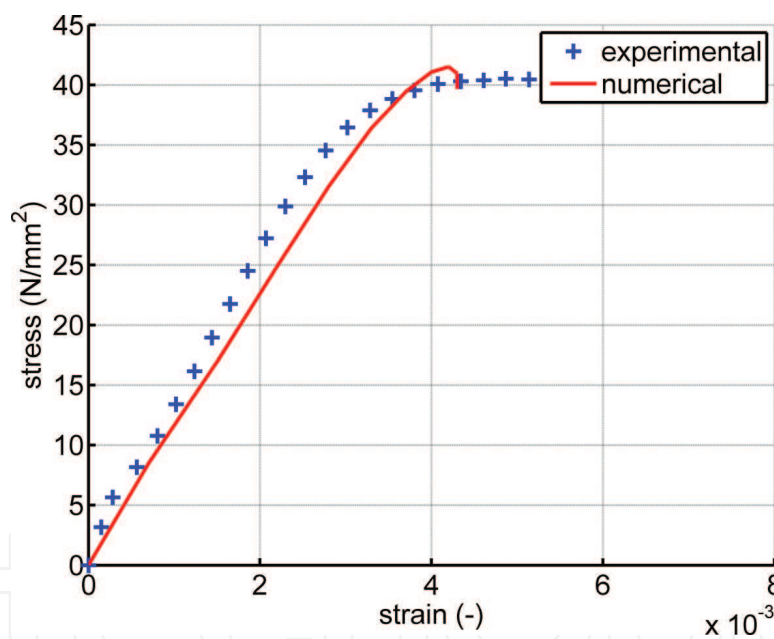

Figure 1. Comparison between numerical and experimental data of the stress-strain path for the compression test, under loading along the longitudinal axes.

Also the numerical results concerning the compression test are reported as a plot of coloured iso-map. These iso-maps show the intensity distribution of displacement, stress, strain and equivalent plastic (inelastic) strain along the longitudinal fibre, at some prefixed time steps (**Figures 2–5**).

In the plotted iso-map of the displacement field, along the longitudinal axes of the specimen (**Figure 2**), it is quite clear to observe the different levels of displacement along the specimen height, it varies from the maximum level at the top edge of the specimen to the minimum at the bottom edge, close to the restrains.
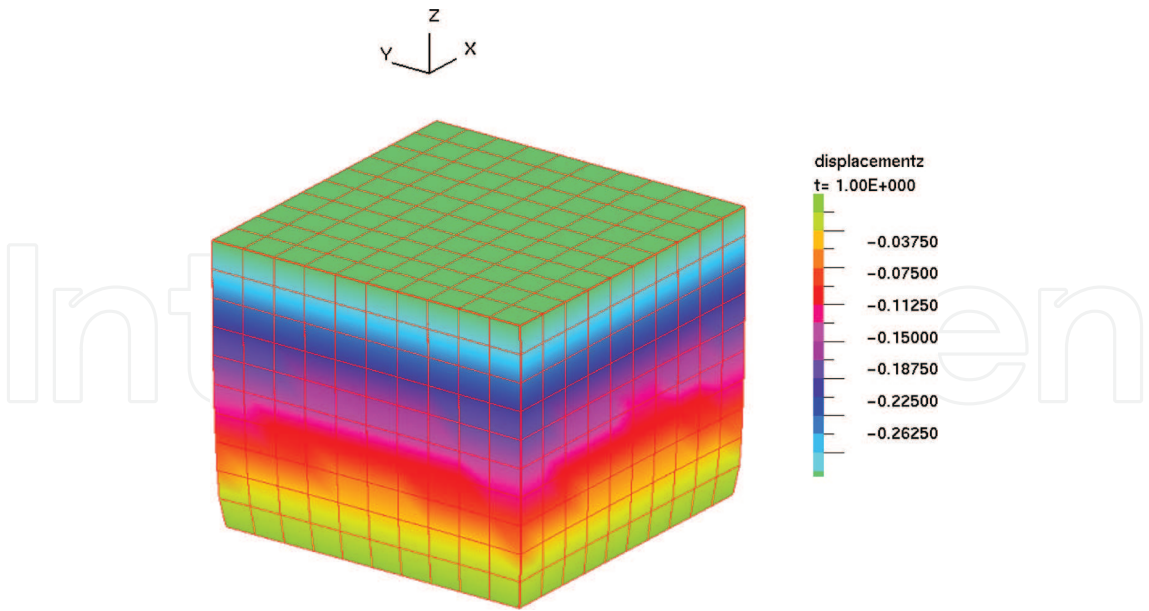
Figure 2. Compression test with the specimen loaded along the longitudinal axes. Plot of the iso-map of the displacement field.

Figure 3 shows the distribution of normal stress along the longitudinal axes of the specimen. The distribution is reasonably uniform with the exception around the edge restrain, where the marked colour variation points out the expected stress concentrations.
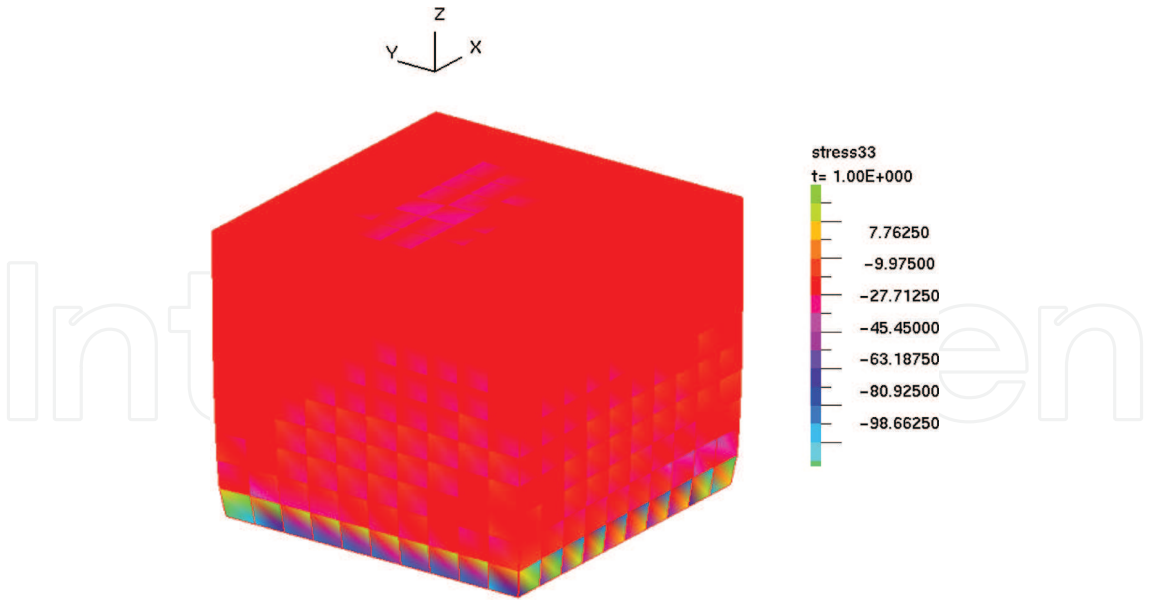

Figure 3. Compression test with the specimen loaded along the longitudinal axes. Plot of the iso-map of the stress field along the longitudinal axes.

Figure 4 displays the colour iso-map of the strain field along the longitudinal axes of the specimen. In this figure, the different levels of strain along the height of the specimen are quite

evident, from a minimum at the bottom edge, which is cinematically restrained, to a maximum at the top, where the deformation increases from the inner side towards the outer side of the specimen.
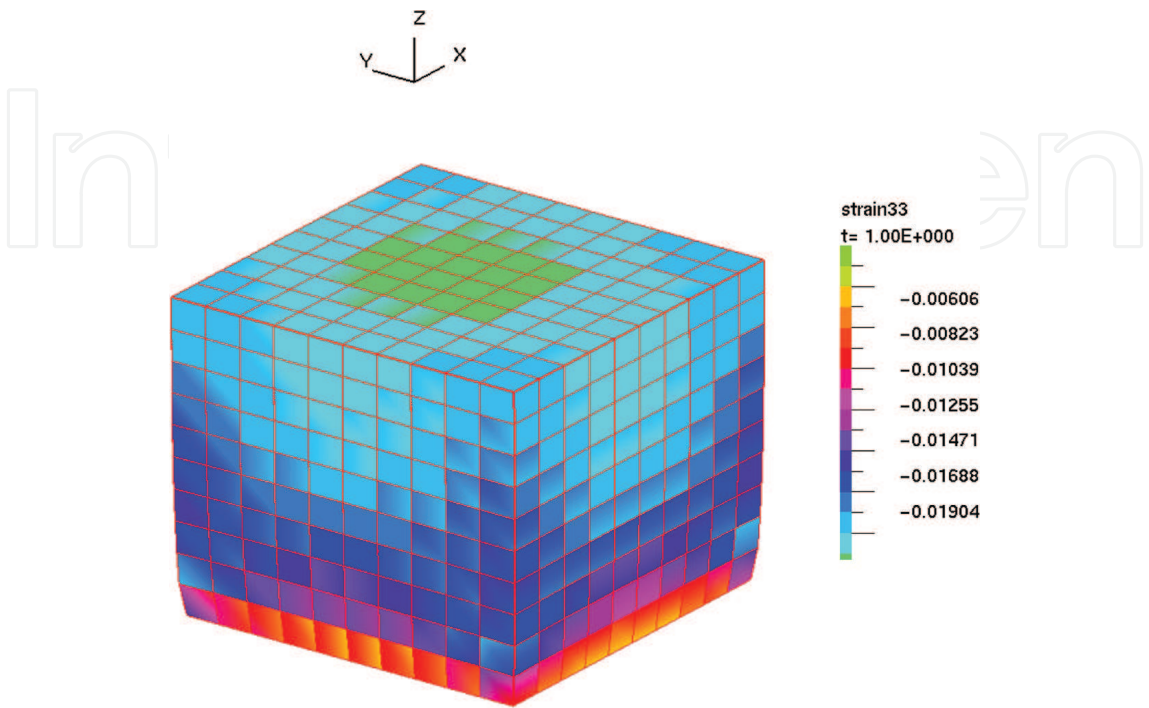

Figure 4. Compression test with the specimen loaded along the longitudinal axes. Plot of the iso-map of the strain field along the longitudinal axes.
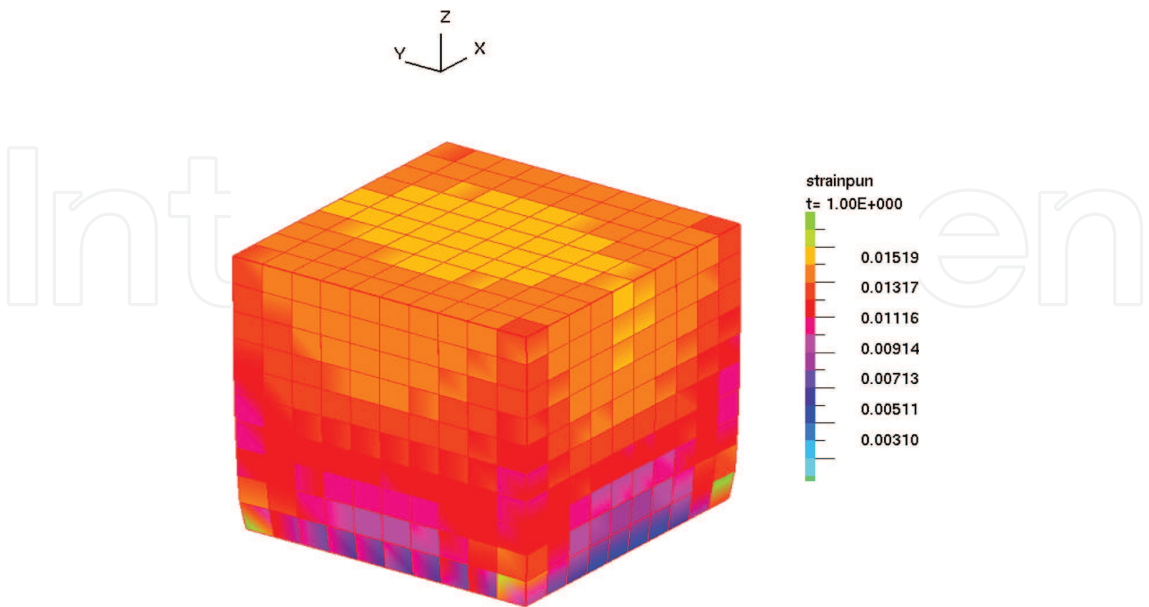

Figure 5. Compression test with the specimen loaded along the longitudinal axes. Plot of the iso-map of the equivalent plastic (inelastic) strain field.

Figure 5 shows the equivalent plastic strain distribution on the specimen shape, which is however comprehensive of other inelastic strains, such as creep. At the loading step illustrated in this figure, the plastic strain is quite extended on the whole of the specimen shape.

The numerical results for the specimen under tension loading are also reported as a plot of coloured iso-map. The iso-maps show the intensity distribution of displacement, stress and strain along the longitudinal fibre, at some prefixed loading stepping (**Figures 6–8**).

Figure 6 shows the displacement field along the longitudinal axes of the specimen. The distribution is quite coherent with a mechanical behaviour, it varies along the height of the specimen with a high level towards the centre of the specimen.
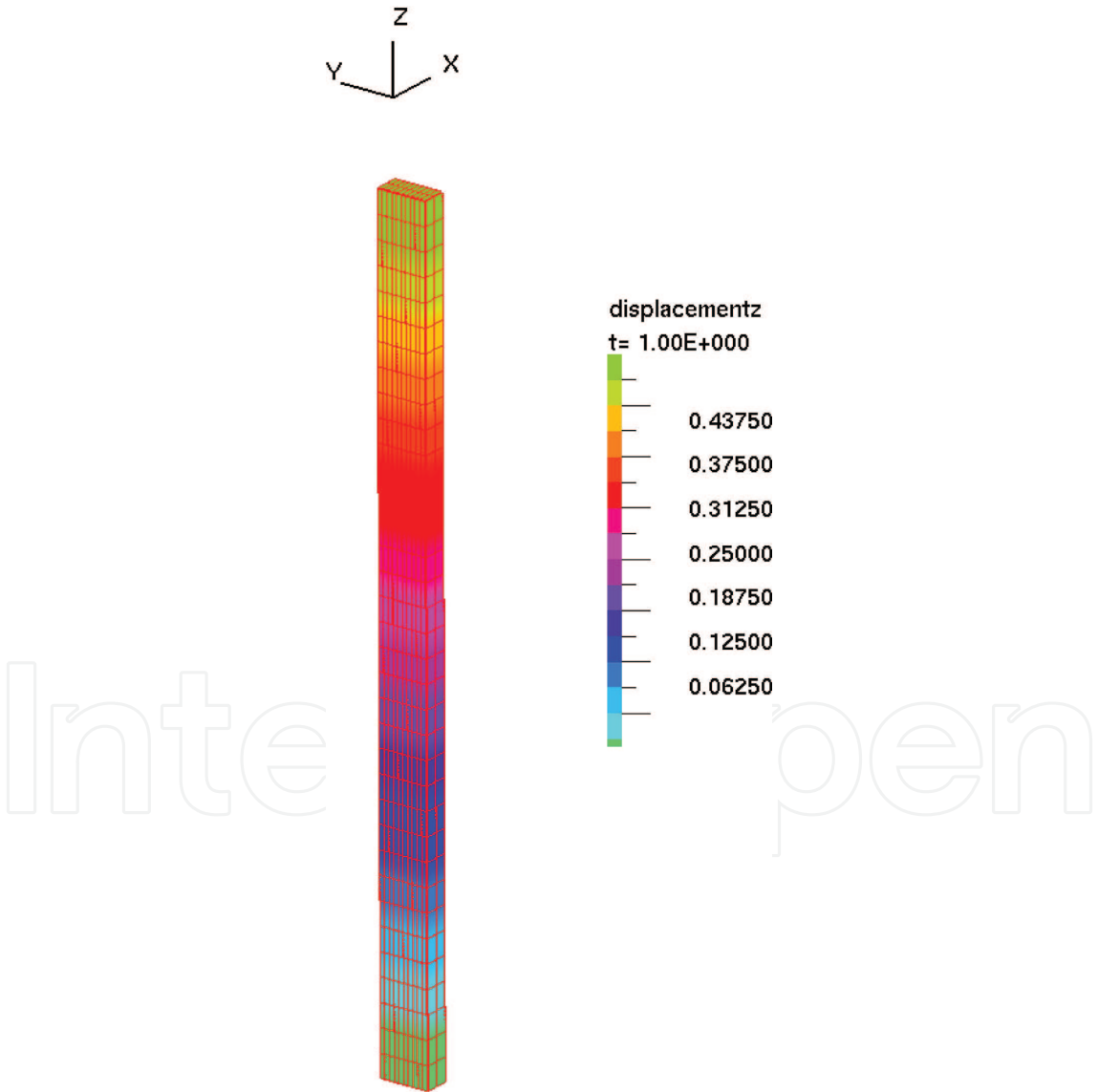

Figure 6. Tension test with the specimen loaded along the longitudinal axes. Plot of the iso-map of the displacement field.

In **Figure 7**, the stress distribution along the longitudinal axes of the specimen is displayed. The distribution is correctly rather uniform. It also presents stress concentrations near the bottom edge where the specimen is held back.

Figure 8 displays the strain iso-map along the longitudinal axes of the specimen. This distribution is quite uniform except near the bottom edge of the specimen.
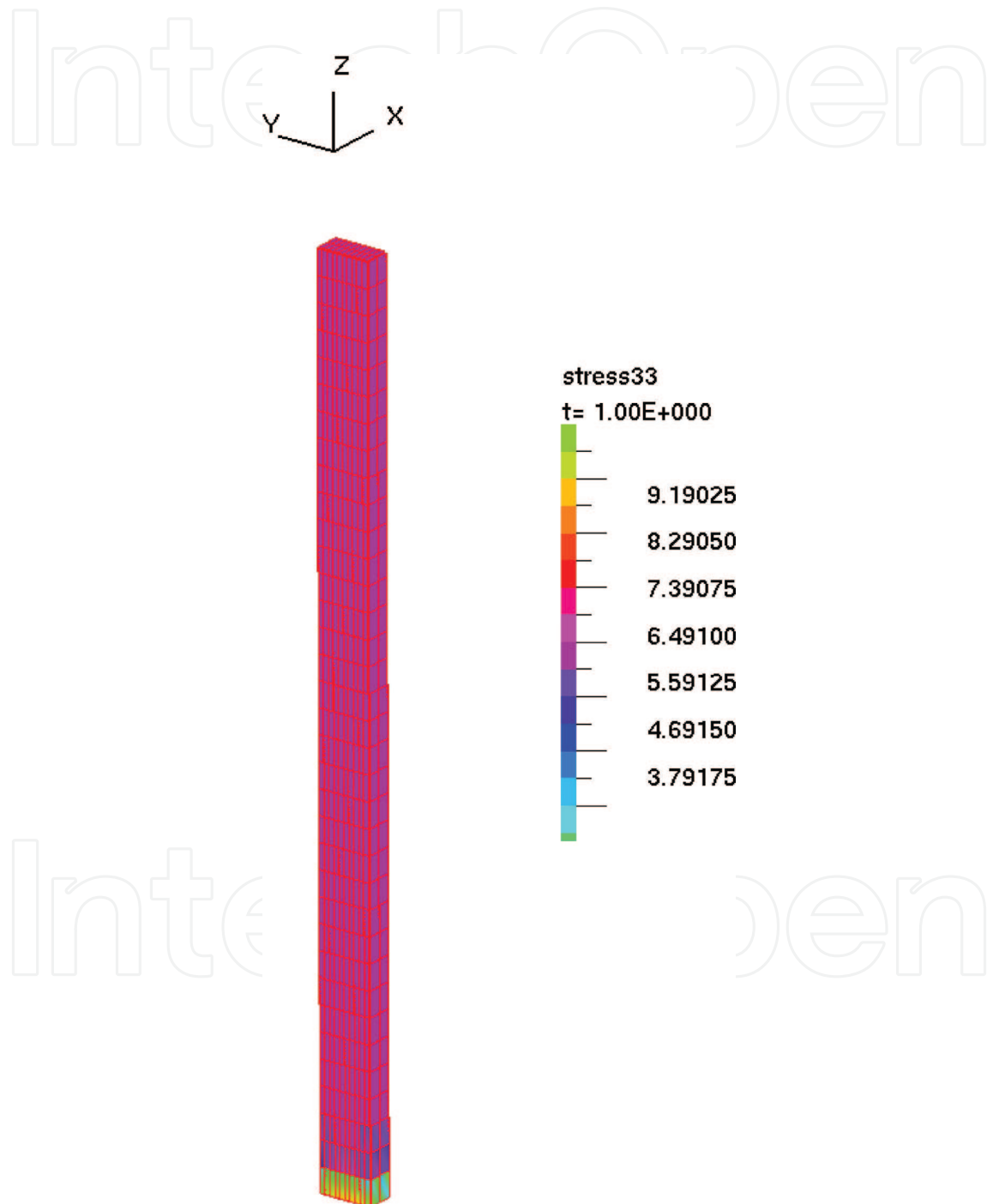

Figure 7. Tension test with the specimen loaded along the longitudinal axes. Plot of the iso-map of the stress field along the longitudinal axes.
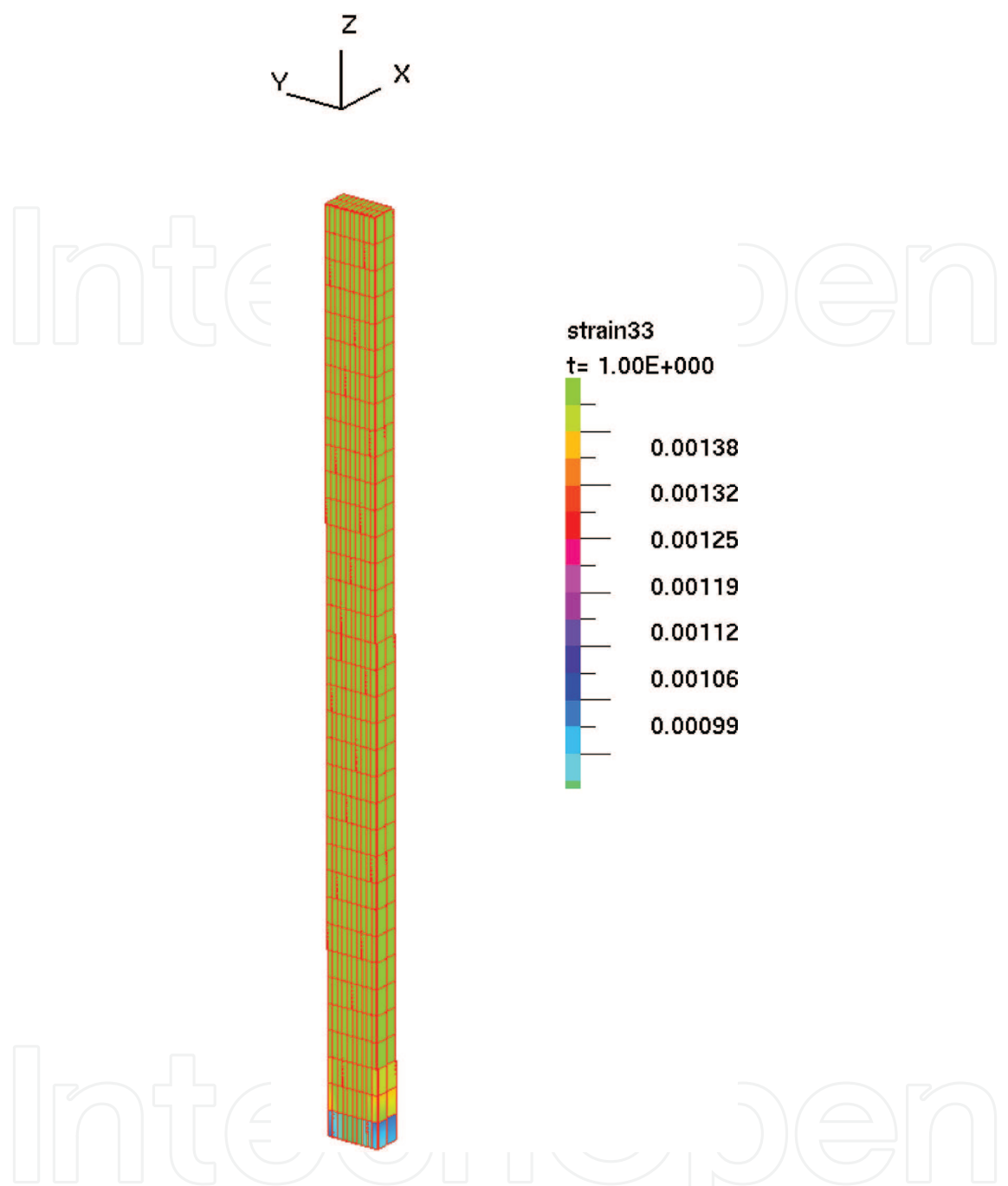
Figure 8. Tension test with the specimen loaded along the longitudinal axes. Plot of the iso-map of the strain field along the longitudinal axes.

4. Conclusions

Most common models, used to analyse the mechanical behaviour of timber or wood composite structures, mainly adopt a single equivalent yield surface to describe the non-linearity of the material. In the present approach a multi-surface yielding description of the non-linear behaviour of wood is proposed. It performs a general orthotropic elastic-viscous-plastic constitutive formulation, according to the finite strain theory. Within a continuum mechanics approach, the

proposed three-dimensional FEM model is capable to represent elastic-viscous-plastic in compression and elastic-brittle in tension behaviour of wood.

On the basis of a preliminary comparison of the numerical results with experimental data, the model has demonstrated to be valuable to represent the main mechanical behaviour of a test specimen. The examples presented here illustrate that the FEM model can be adequate to examine the mechanical behaviour of wood under displacement loading both in linear and non-linear situations. The model has been built within a general purpose FEM code, its formulation being quite general it is almost powerful to describe complex states in wood materials such as anisotropy, elasticity and visco-plasticity, brittle crack occurring in the timber structure. However, the validation of the model with the comparison between numerical and experimental results can be carried out in a future work

Acknowledgements

Author details

Vincenzo De Luca

Address all correspondence to: vincenzo.deluca@unibas.it

Dipartimento DIS, Università degli Studi della Basilicata, Potenza, Italy

References

[1] De Luca V., Marano C. Prestressed glulam timbers reinforced with steel bars. Construction and Buildings Materials. 2012; **30**:206–217. DOI: 10.1016/j.conbuildmat.2011.11.016.

[2] Patton-Mallory M., Cramer S. M., Smith F. W., Pellicane P. J. Nonlinear material models for analysis of bolted wood connections. Journal of Structural Engineering. 1997; **123(8):**1063–1070.

[3] Perkins R. W. Concerning the mechanics of wood deformation. Forest Production Journal. 1967; **17**(3):55–67.

[4] Bodig J., Jayne B. A. Mechanics of wood and wood composites. New York, USA: Van Nostrand Reinhold Company; 1982.

[5] Dinwoodie J. M. Timber—its nature and behaviour. New York, NY: Van Nostrand Reinhold Company; 1981.

[6] De Luca V., Sabia D. Mechanical compression tests to model timber structures behaviour. In: A. A. Mammoli and C. A. Brebbia, editor. Computational Methods and Experiments

in Materials Characterization III. WIT Transaction on Engineering Sciences; 13 June 2007 through 15 June 2007; Bologna (Italy). Southampton: WIT Press. Southampton; 2007. Volume 57 pp. 273–278. DOI: 10.2495/MC070271.

[7]   Hankinson R. L. Investigation of Crushing Strength of Spruce at Varying Angles of Grain. Air Service Information Circular No. 259, U. S. Air Service; 1921.

[8]   Goodman J. R., Bodig J. Orthotropic strength of wood in compression. Wood Science. 1971; **4**(2):83–94.

[9]   Tsai S. W., Wu E. M. A general theory of strength for anisotropic materials. Journal of Composite Materials. 1971; **5**:58–80.

[10]   Tabiei A., Wu J. Three-dimensional nonlinear orthotropic finite element material model for wood. Composite Structures. 2000; **50**:143–149.

[11]   Schmidt J., Kaliske M. Models for numerical failure analysis of wooden structures. Engineering Structures. 2009; **31**:571–579. DOI: 10.1016/j.compstruc.2011.06.004.

[12]   Oudjene M., Khelifa M. Finite element modelling of wooden structures at large deformations and brittle failure prediction. Materials and Design. 2009; **30**:4081–4087.

[13]   Dahl K. B., Malo K. A. Nonlinear shear properties of spruce softwood: numerical analyses of experimental results. Composites Science and Technology. 2009; **69**:2144–2151.

[14]   Oudjene M., Khelifa M. Elasto-plastic constitutive law for wood behaviour under compressive loadings. Construction and Building Materials. 2009; **23**:3359–3366.

[15]   Khennane A., Khelifa M., Bleron L., Viguier J. Numerical modelling of ductile damage evolution in tensile and bending tests of timber structures. Mechanics of Materials. 2014; **68**:228–236.

[16]   De Luca V., Della Chiesa A. A creep non-linear FEM analysis of glulam timber. Mechanics of Advanced Materials and Structures. 2013; **20**:489–496. DOI: 10.1080/15376494.2011. 627643.

[17]   Moayyed M. Y, Taheri F. Creep response of glulam reinforced by a novel pre-stressed FRP-wood composite system. 11th World Conference on Timber Engineering 2010 (WCTE 2010), Trentino, Italy, 20–24 June, 2010.

[18]   Bathe K. J. Finite element procedures. Upper Saddle River: Prentice Hall; 1995.

[19]   Zienkiewicz O., Taylor R. The finite element method. Volume 1: The basis. Oxford: Butterworth-Heinemann; 2000.

[20]   Zienkiewicz O., Taylor R. The finite element method. Volume 2: Solid mechanics. Oxford: Butterworth-Heinemann; 2000.

[21]   Carosio A., Willam K., Etse G. On the consistency of viscoplastic formulations. International Journal of Solids and Structures. 2000; **37**:7349–7369.

[22] De Angelis F. On the structural response of elasto/viscoplastic materials subject to time-dependent loadings. SDHM Structural Durability and Health Monitoring. 2012; **8** (4):341–358.

[23] De Angelis F. Numerical algorithms for j2 viscoplastic models. Advanced Materials Research. 2012; **567**:267–274. DOI: 10.4028/www.scientific.net/AMR.567.267

[24] De Angelis F. Computational aspects in the elasto/viscoplastic material behavior of solids. Advanced Materials Research. 2012; **567**:192–199. DOI: 10.4028/www.scientific.net/AMR.567.192

[25] De Angelis F. On constitutive relations in non-smooth elasto/viscoplasticity. Advanced Materials Research. 2012; **566**:691–698. DOI: 10.4028/www.scientific.net/AMR.566.691

[26] De Angelis F. Computational issues in rate-dependent plasticity models. Advanced Materials Research. 2012; **566**:70–77. DOI: 10.4028/www.scientific.net/AMR.566.70.

[27] Simo J. C., Ortiz M. A unified approach to finite deformation elastoplastic analysis based on the use of hyperelastic constitutive equations. Computer Methods in Applied Mechanics and Engineering. 1985; **49**:221–245.

[28] Moran B., Ortiz M., Shih. C. F. Formulation of implicit finite element methods for multiplicative finite deformation plasticity. International Journal for Numerical Methods in Engineering. 1990; **29**:483–514.

[29] Wang W. M., Pozivilova A., Sluys L. J. Implicit algorithms for finite deformation viscoplasticity. European Congress on Computational Methods in Applied Sciences and Engineering, ECCOMAS 2000, Barcelona 11–14 September, 2000.

[30] Wang W. M., Sluys L. J. Formulation of an implicit algorithm for finite deformation viscoplasticity. International Journal of Solids and Structures. 2000; **37**: 7329–7348.

[31] García Garino C., Ribero Vairo M. S., Andía Fagés S., Mirasso A. E., Ponthot J.-P. Numerical simulation of finite strain viscoplastic problems. Journal of Computational and Applied Mathematics. 2013; **246**:174–184. DOI: 10.1016/j.cam.2012.10.008.

[32] Cuitino A. M., Ortiz M. A. A material-independent method for extending stress update algorithms from small-strain plasticity to finite plasticity with multiplicative kinematics. Engineering Computations. 1992; **9**:437–451.

[33] Rodríguez-Ferran A., Pegon P., Huerta A. Two stress update algorithms for large strains: accuracy analysis and numerical implementation. International Journal for Numerical Methods in Engineering. 1997; **40**(23):4363—4404.

[34] Lubliner J Plasticity theory. First ed. New York, USA: Macmillan Publishing Company; 1990.

[35] Eidel B., Gruttmann F. Elastoplastic orthotropy at finite strains: multiplicative formulation and numerical implementation. Computational Materials Science. 2003; **28**:732–742.

[36] Holmes D. W., Loughran J. G. Numerical aspects associated with the implementation of a finite strain, elasto-viscoelastic–viscoplastic constitutive theory in principal stretches.

International Journal for Numerical Methods in Engineering. 2010; **83**:366–402. DOI: 10.1002/nme.2850.

[37] Schröder J., Gruttmann F., Löblein J. A simple orthotropic finite elasto–plasticity model based on generalized stress–strain measures. Computational Mechanics. 2002; **30**:48–64. 10.1007/s00466-002-0366-3.

[38] Forest Product Laboratory (FPL). Wood handbook-wood as an engineering material. General Technical Report FPL-GTR-113. Madison (WI, USA): Department of Agriculture; 1999.

[39] Lekhnitskii S. G. In: Brandstatter J. J., editor. Theory of elasticity of an anisotropic elastic body. San Francisco, CA: Holden Day, Inc.; 1963.